Box–Behnken Design for Optimizing Synthesis and Adsorption Conditions of Covalently Crosslinked Chitosan/Coal Fly Ash Composite for Reactive Red 120 Dye Removal

Ibrahim Awad Mohammed[1,2] · Nurul Najwa Abd Malek[1] · Ali H. Jawad[1] · Mohd Sufri Mastuli[1,3] · Zeid A. ALOthman[4]

Abstract

In this research, a biocomposite adsorbent of covalently crosslinked chitosan-epichlorohydrin/coal fly ash (CHT-ECH/CFA) was synthesized and applied for reactive red 120 dye (RR120) removal. The CHT-ECH/CFA was characterized by BET, pH potentiometric, pH_{pzc}, XRD, FTIR and SEM-EDX. A statistical optimization by Box–Behnken Design (BBD) was employed to assess the effects of the adsorption key parameters such as CFA loading into CTH-ECH matrix, adsorbent dose, solution pH, working temperature and contact time. The optimized CFA loading, adsorbent dose, temperature, time, and pH were observed to be 50%, 0.07 g, 45 °C, 60 min, and solution pH 4 respectively. From BBD, the highest removal of RR120 at optimum operation conditions was found to be 90.2%. The experimental results show the adsorption process can be perfectly described by both Langmuir and Freundlich isotherm models with maximum adsorption capacity of 237.7 mg/g at 45 °C. Moreover, the adsorption kinetics were well fitted to the pseudo-second order model. This research introduces a new hybrid biocomposite adsorbent with potential application for the treatment of anionic dye-polluted water.

Keywords Box-Behnken design · Crosslinked chitosan · Coal fly ash

Introduction

Industrialization and urbanisation have benefited the society in different ways. However, releasing a large amount of polluted water with dyes into natural water system is like a two-edged sword. The presence of colour remnants, industrial dyes, catalytic chemicals and inorganic matters in the wastewater originating from textile, printing inks, fluorescent lamp, plastic and tanning industries are regarded as serious and formidable threats [1]. The disastrous emergence in these industries has left a wide environmental footprint, with chemicals employed in their manufacturing lines potentially escaping into the adjacent waterways [2]. Among various types of discharged dyes, the azo group and anthraquinone containing dyes comprise approximately 70% and 15%, respectively. Reactive Red 120 (RR 120) is an example of the azo dyes that is commonly used in the textile industries due to their uncomplicated dying practices and desirable stability during the wash-off process. Thus, RR120 has high chemical stability, low biological degradability and poses a risk to humans and the eco-system [3, 4]. Therefore, as a result of the growing awareness concerning the adverse effects of dyes in water, the industries are compelled to meet the requirements of increasingly stringent regulations promulgated by governments and regulatory bodies [5].

Chitosan (CHT) is a polymer containing hydroxyl (–OH) and amino (−NH₂) functional groups, these functional groups make CHT as a benchmark adsorbent due to its potential ability for removing a wide range of pollutants such as heavy metal ions [6], pharmaceutical compounds [7] and dyes [8]. The availability of the abundance of amino and hydroxyl groups in CHT backbone are not only essential for a strong electrostatic attraction for capturing various water contaminants. Consequently, these functional groups can

✉ Ali H. Jawad
ali288@uitm.edu.my; ahjm72@gmail.com

1 Faculty of Applied Sciences, Universiti Teknologi MARA, 40450 Shah Alam, Selangor, Malaysia

2 College of Dentistry, Kirkuk University, Kirkuk City, Iraq

3 Centre for Functional Materials & Nanotechnology, Institute of Science, Universiti Teknologi MARA, 40450 Shah Alam, Selangor, Malaysia

4 Chemistry Department, College of Science, King Saud University, 11451 Riyadh, Saudi Arabia

serve as excellent binding sites to modify and upgrade CHT for any desirable purpose [9]. However, direct application of pristine CHT in wastewater treatment technologies is not preferable due to its high swelling capacity and poor chemical stability in acidic environment. Therefore, the physical and chemical modification of CHT is not a dispensable option for enhancing its chemical stability and adsorptive property.

Thus, selection of the right modification method and choosing the right modifying agent is a very important issue to determine the quality and functionality of the synthesised CHT product. In this regard, there are plenty of nano scale organic/inorganic fillers that have been utilized to improve the surface area property, chemical stability, thermal stability, functionality, and adsorptive performance such as nano titania [8], magnesium oxide [10], silica [11], kaolin [12], magadiite [5], zinc oxide [13], and graphene nanoplates [14]. On the other hand, crosslinking process is a very demanded approach to improve the chemical stability, functionality, and hydrophobicity of CHT by forming an irreversible network with either (–OH) or (–NH$_2$) functional groups of CHT, and it depends on the nature and chemical structure of the crosslinked agent.

For instance, glutaraldehyde (GLA) is the benchmark dialdehyde crosslinked agent that binds covalently with CHT's amino group (–NH$_2$) at C-3 position to form Schiff's-base system and as a result, improving mechanical performance and chemical stability of CHT [1]. In fact, amino (–NH$_2$) group is the prime active adsorption site in the CHT backbone, especially when the CHT is very much needed for removal of anionic species from contaminated water [15]. Therefore, it is hypothesized that finding an alternative crosslinker agent that interacts covalently with $-$OH group at C-6 in the CHT backbone may present the same inserting physicochemical properties as CHT-GLA, while avoiding the shortcomings of making amino ($-$NH$_2$) sites occupied to result in preferable adsorption performance [16]. To avoid any reduction in the adsorption capacity of crosslinked CHT's derivative, choosing epichlorohydrin (ECH) as an epoxy chloropropane (C$_3$H$_5$ClO) crosslinker agent that interacts only with the $-$OH group in CHT backbone will overcome this operation issue.

Coal fly ash (CFA) which is a fine ash collected from the flue gas after coal combustion is the primary solid waste emitted from thermal power stations [17]. By following the principles of the circular economy, recycling the CFA will reduce the landfill pressure and accomplish the idea of waste-free production, paving the way for sustainable reuse of an industrial byproduct [18]. As a typical aluminosilicates material with particle size varying from 1 to 100 µm, CFA is mainly composed of SiO$_2$, Al$_2$O$_3$, Fe$_2$O$_3$ and CaO [19]. Thus, CFA is predominantly utilized to manufacture bricks, cement additives, concrete blocks and other construction

materials [20]. In terms of high-value added material, efforts have been devoted on its possible utilizations as an adsorbent to remove various pollutants from aqueous system [21, 22]. Based on the above-mentioned interesting properties of CHT and CFA, it can be anticipated that CHT and CFA can complement each other with their own advantages to develop a hybrid composite of CHT-CFA with unique surface property for potential application.

Thus, there are many interesting works have been done on developing CHT-CFA composite based materials for various potential applications such as flocculant [23], magnetic chitosan -fly ash for cellulase immobilization and bioconversion [24], chitosan/polydopamine@C@magnetic fly ash for silver removal from aqueous environment [25], fly ash coated chitosan for removal of chromium, copper, zinc and arsenic [26], chitosan/NaOH/fly ash for removal of tannic acid [27], ionic cross-linked chitosan-fly ash with tripolyphosphate for reactive dye removal [28]. Although the literatures have highlighted the efficiency of CHT/CFA based materials in those applications, however, the application of statistical optimization for synthesis conditions and other operating key parameters are not much involved in those research projects.

Therefore, the main objective of this study is to produce crosslinked chitosan-epichlorohydrin with coal fly ash and to produce a hybrid crosslinked chitosan-epichlorohydrin/coal fly ash (CHT-ECH/CFA) biocomposite as a promising hybrid adsorbent for removal of reactive red (RR120) dye from aqueous environment. Box–Behnken design in response surface methodology was applied to optimize the synthesis and adsorption characteristics of CHT-ECH/CFA as a function of process parameters namely CFA loading, adsorbent dose, solution pH, working temperature, and contact time. The regression analysis was performed to investigate the fitness of the experimental data to full-quadratic model with a coefficient of determination (R^2). Moreover, the adsorption kinetic, isotherm, thermodynamic, and mechanism of RR120 by CHT-ECH/CFA were discussed.

Materials and Methods

Materials

Chitosan (CHT) (deacytelation $\geq$ 75%; medium molecular weight) and epichlorohydrin (ECH) were purchased from Sigma-Aldrich. A thermal power plant in Kapar, Klang, Selangor, Malaysia provided the coal fly ash (CFA) powder in micro scale particles [29]. Reactive Red 120 (RR120) (formula weight: C$_{44}$H$_{24}$C$_{12}$N$_{14}$O$_{20}$S$_6$Na$_6$, molecular weight: 1469.98, λmax: 534 nm) was procured from Sigma-Aldrich.

Synthesis of CHT-ECH/FA

1 g of CHT was dissolved in 50 mL of 5% acetic acid solution and left to stir overnight until homogenized. The CHT beads were then prepared by injecting the CHT solution into 100 mL of 0.5 M NaOH. CHT beads were then washed thoroughly with distilled water to remove NaOH residues. The step of crosslinking was performed by adding 100 mL of 2% ECH to the CHT beads and stirred for 2 h at 40 °C. The CHT-ECH beads were washed with distilled water and air dried. Lastly, the CHT-ECH beads were converted into powder form with a constant particle size of ≤ 250 µm and the powder was kept in an airtight container. Different ratios of CFA_{25} (25% CFA: 75% CHT), and CFA_{50} (50% CFA: 50 CHT) were loaded into polymeric matrix of CHT using the same process described above. Except that the CFA particles were mixed physically with CHT before being added to the acetic acid solution. The same steps described above were adopted for crosslinking. The composite with constant loading ratio of 25% CFA and 50% CFA were labelled as CHT-ECH/CFA_{25} and CHT-ECH/CFA_{50}, respectively. The materials were further ground and sieved to constant particle size of ≤ 250 µm.

Samples Characterization

The morphological characteristics of the CHT-ECH/CFA were analysed using a scanning electron microscope equipped with energy dispersive X-ray analyser (SEM-EDX, Hitachi TM3030 Plus). The surface of CHT-ECH/CFA was sputter-coated with gold before imaging. The chemical structure of the CHT-ECH/CFA was identified using FTIR Spectroscopy (Perkin-Elmer, Spectrum RX1) in the range of 4000 cm^{-1}–450 cm^{-1} applying the KBr pellet technique. The X-ray diffraction (XRD) patterns of CHT-ECH/CFA were obtained by using X'Pert PRO, PANalytical Cu Kα radiation ($\lambda = 1.54$ Å). The estimation of amino (–NH_2) content in CHT-ECH/CFA was made using the pH-potentiometric titration method as described by Vieira and Beppu [30]. The determination of point of zero charge (pH_{pzc}) of the CHT, CFA, and their composite form of CHT-ECH/CFA was done according to the published method [31].

Design of Experiment

Response surface methodology (RSM) coupled with Box-Behnken design (BBD) was applied to design the experiments and to perform the statistical analysis using Design expert software (version 13.0). A three-level, five-factor Box-Behnken design was applied in this study. The investigated independent variables, CFA loading (%) (A), adsorbent dose (B), solution pH (C), working temperature (D), and contact time (E) with their coded levels −1 (minimal),

0 (central point) and + 1 (maximal) are listed in Table 1. Consequently, BBD contains forty-six sets of experiments (40 factorial points and 6 centre points) which were conducted. Table 2 presents experimental design and test results of response (RR120 removal (%)). The obtained results were statistically evaluated by quadratic response surface Eq. (2nd degree polynomial equation) as expressed in Eq. (1) [32].

$$Y = \beta_0 + \sum \beta_i X_i + \sum \beta_{ii} X_i^2 + \sum \sum \beta_{ij} X_i X_{j+} \epsilon o \qquad (1)$$

where 'Y' is the predicted response (RR120 removal (%)); 'X_i' and 'X_j' are independent variables; 'β_o', 'β_i', 'β_{ii}', 'β_{ij}' are coefficient of regression; 'k' is the dimensional space; 'ε_o' is the noise or error observed in the predicted responses. Then, the statistical fitness and significance of the model were assessed using Analysis of Variance (ANOVA) (F-value and p-value). The high model F-value and low p-value of the model ($P < 0.05$) indicate the statistical significance of the model [32].

Response Determination (RR120 Removal %)

The determination of response (RR120 removal (%)) was experimentally performed by transferring 100 mL RR120 dye solution of 50 mg/L into a 250 mL conical flask. A desired amount of the specific adsorbent (CHT-ECH, CHT-ECH/CFA_{25}, CHT-ECH/CFA_{50}) was weighed and transferred to the flasks. In thermostat water bath shaker (WNB7–45, Memmert, Germany), these flasks were stirred at a constant stirring rate of 100 strokes/min. After completing the adsorption process, the filtration process for adsorbent/adsorbate system was carried out using a 0.45 µm syringe filter to filter the residual solution. Lastly, the concentration of RR120 was monitored at λ_{max} of 534 nm using HACH DR 3900, a UV-Vis spectrophotometer. The RR120 dye removal (DR %) was determined according to Eq. 2.

$$DR\% = \frac{C_o - C_e}{C_o} \times 100 \qquad (2)$$

C_o (mg/L) is the initial concentration of RR120 dye and C_e (mg/L) is the equilibrium concentration of the RR120 dye

Table 1 Codes and actual ranges of independent variables and their levels

Codes	Variables	Level 1 (−1)	Level 2 (0)	Level 3 (+ 1)
A	CFA loading (%)	0	25	50
B	Dose	0.04	0.07	0.10
C	pH	4	7	10
D	Temperature (°C)	30	45	60
E	Time (min)	30	60	90

Run	A: CFA loading (%)	B: Dose (g)	C: pH	D: Temp. (°C)	E: Time (min)	RR 120 removal (%)
1	0	0.04	7	45	60	23.6
2	50	0.04	7	45	60	49.4
3	0	0.1	7	45	60	31.5
4	50	0.1	7	45	60	83.2
5	25	0.07	4	30	60	38.2
6	25	0.07	10	30	60	28.1
7	25	0.07	4	60	60	60.9
8	25	0.07	10	60	60	27.6
9	25	0.04	7	45	30	18.6
10	25	0.1	7	45	30	47.2
11	25	0.04	7	45	90	35.2
12	25	0.1	7	45	90	50.1
13	0	0.07	4	45	60	34.6
14	50	0.07	4	45	60	90.2
15	0	0.07	10	45	60	12.7
16	50	0.07	10	45	60	47.9
17	25	0.07	7	30	30	27.1
18	25	0.07	7	60	30	55.2
19	25	0.07	7	30	90	52.2
20	25	0.07	7	60	90	53.1
21	25	0.04	4	45	60	43.9
22	25	0.1	4	45	60	61.1
23	25	0.04	10	45	60	27.9
24	25	0.1	10	45	60	33.1
25	0	0.07	7	30	60	29.4
26	50	0.07	7	30	60	50.6
27	0	0.07	7	60	60	44.1
28	50	0.07	7	60	60	74.1
29	25	0.07	4	45	30	45.7
30	25	0.07	10	45	30	18.9
31	25	0.07	4	45	90	52.4
32	25	0.07	10	45	90	29.4
33	0	0.07	7	45	30	21.1
34	50	0.07	7	45	30	65.3
35	0	0.07	7	45	90	42.8
36	50	0.07	7	45	90	70.6
37	25	0.04	7	30	60	24.3
38	25	0.1	7	30	60	34.8
39	25	0.04	7	60	60	29.1
40	25	0.1	7	60	60	61.5
41	25	0.07	7	45	60	35
42	25	0.07	7	45	60	32.5
43	25	0.07	7	45	60	30.3
44	25	0.07	7	45	60	33.1
45	25	0.07	7	45	60	25.1
46	25	0.07	7	45	60	30.8

Table 2 The 4-variable BBD matrix and experimental data for RR120 removal (%)

Batch Adsorption Study

In this study, the batch adsorption mode was adopted to figure out the effect of initial RR120 concentration and contact time on the removal of RR120 using the optimal key adsorption parameters obtained from run 14 of BBD as listed in Table 2. These optimum adsorption conditions were implemented in the adsorption study using a conical flask (250 mL) with 100 mL of RR120 dye at different series of initial concentrations ranging from 50 to 300 mg/L. The adsorbed amount of the RR120 was quantified using Eq. 3.

$$q_e = \frac{(C_o - C_e)V}{W} \qquad (3)$$

q_e (mg/g) is the adsorption capacity at equilibrium, W (g) is the mass of the adsorbent and V (L) is the volume of RR120 dye solution.

Results and Discussion

Samples Characterization

The specific surface area and other physical parameters of the CHT-ECH, CHT-ECH/CFA$_{25}$, and CHT-ECH/CFA$_{50}$ are summarized in Table 3. From the results, it is proven that the specific surface area (BET), Langmuir surface area, t-Plot external surface area, and total pore volume of CHT-ECH were improved gradually by increasing the loading of CFA in the polymeric matrix of CHT-ECH from 25 to 50%, signifying the significant role of the CFA in enhancing the surface area and pore diameter of CHT-ECH, and subsequently improving its adsorption property.

Opposite to specific surface area trend, the actual content of amino (–NH$_2$) group in the polymeric matrix of the CHT-ECH/CFA$_{50}$ shows the lowest content (22.05%) compared to CHT-ECH/CFA$_{25}$ (29.23%), and CHT-ECH (45.24%) as presented in Table 3. These expected results can be assigned to contribution of the CFA content in the polymeric matrix of the composite CHT's derivative. In other words, when the ratio of CFA increased in the CHT-ECH-CFA formulation,

correspondingly the CHT content will be less according to the desired mixing ratio, consequently the amino (–NH$_2$) group will be less. However, amino (–NH$_2$) group content (22.05%) in the polymeric matrix of CHT-ECH/CFA$_{50}$ is still preferable with high potential to serve as active sites for adsorption after protonation process [33]. The results of the pH$_{pzc}$ analysis are presented in Table 3. As recorded in Table 3, the pH$_{pzc}$ values of the CHT-ECH, CFA, and CHT-ECH/CFA$_{50}$ were found to be 7.9, 8.9, and 7.1 respectively.

The XRD patterns of CHT-ECH, CHT-ECH/CFA$_{25}$, CHT-ECH/CFA$_{50}$ are presented in Fig. 1. As can be seen from Fig. 1a, a broad hump around $2\theta = 20.5°$ is a signature peak for CHT biopolymer [34]. After loading 25% of CFA microparticles (CHT-ECH/CFA$_{25}$), new distinguished peaks with different intensities appear at $2\theta = 26°$, 35°, and 43° as shown in Fig. 1b. This observation confirms the loading and uniform distribution of the CFA microparticles in the polymeric matrix of CHT-ECH, and predominantly composed of crystalline phases such as hematite, quartz, and alumina. Besides that, the XRD profile after loading 50% CFA microparticles (CHT-ECH/CFA$_{50}$) is shown in Fig. 1c.
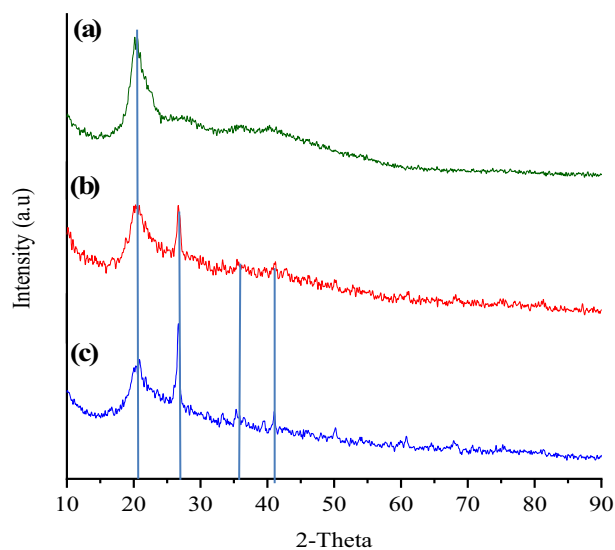
Fig. 1 XRD pattern of (a) CHT-ECH, (b) CHT-ECH/CFA$_{25}$, (c) CHT-ECH/CFA$_{50}$

Table 3 Surface area property and actual amino groups content of prepared samples

Specific surface area	CHT-ECH	CHT-ECH/CFA$_{25}$	CHT-ECH/CFA$_{50}$
BET Surface Area (m²/g)	0.44	1.08	2.12
Langmuir Surface Area (m²/g)	0.54	2.98	4.37
t-Plot external surface area (m²/g)	0.63	1.89	2.23
Average pore diameter (nm)	2.61	5.83	12.73
pH-Potentiometric titration – NH$_2$ (%)	45.24	29.23	22.05
pH$_{pzc}$ analysis	CHT-ECH	CFA	CHT-ECH/CFA$_{50}$
	7.9	8.9	7.1
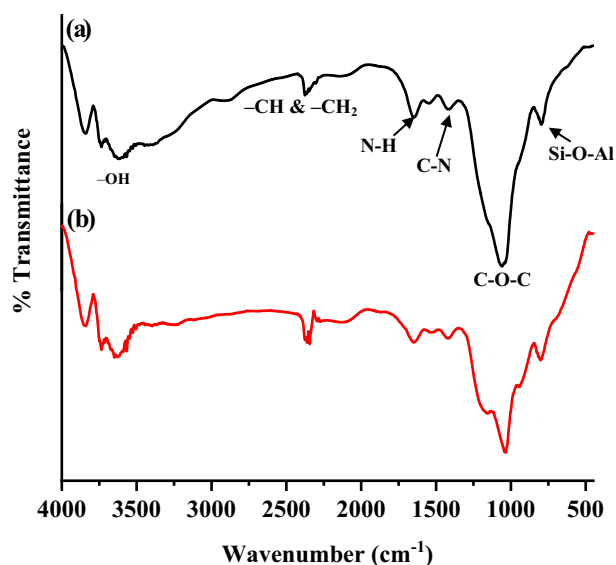
Fig. 2 FTIR spectra of (a) CHT-ECH/CFA$_{50}$, (b) CHT-ECH/CFA$_{50}$ after adsorption of RR120 dye

As can be seen, the spectrum of Fig. 1c is quite similar to the spectrum of Fig. 1b, except the intensity of the distinguished peaks become slightly sharper due to the extra loading of CFA microparticles.

The functional groups present in CHT-ECH/CFA before and after uptake of RR120 were identified using FTIR analysis and displayed in Fig. 2. The band observed for the CHT-ECH/CFA before adsorption at 3600 cm^{-1} can be ascribed to vibrations of –OH, while the band around 2400 cm^{-1} is associated with C–H stretching in –CH and –CH$_2$ [5]. The remaining major bands could be attributed as follows: 1650 cm^{-1} (bending vibration of N–H), 1380 cm^{-1} (stretching vibration of C–N) and 600 cm^{-1} (vibration of Si–O–Al) [29]. The peak at 1040 cm^{-1} corresponds to the vibrations of C–O–C bond, indicating that ECH interacts with the carbon atom of the –OH and CHT to form covalent bonds, resulting in the opening of epoxide ring of ECH and the release of Cl atom [35]. After adsorption of RR120 on CHT-ECH/CFA$_{50}$, slight shifting in some peaks such as C–N stretching, N–H bending and C–O groups was observed, which could suggest the binding of RR120 to the surface of CHT-ECH/CFA$_{50}$ [36].

The morphology and EDX spectra of CHT-ECH, CHT-ECH/CFA$_{25}$, CHT-ECH/CFA$_{50}$ before and after RR120 adsorption are depicted in Fig. 3a and c, respectively. The surface of CHT-ECH appeared as a wavy and compact surface as shown in Fig. 3a. The elements present on the surface as revealed by EDX analysis are C, O, H, and N. However, it can be seen from Fig. 3b, by adding CFA, the surface morphology appeared to be rough with visible cavities. Surface roughness and porosity is an essential factor that affects the efficiency of the adsorption process [37]. The spherical particles of different sizes as highlighted in red

circles, embedded on CHT-ECH/CFA$_{25}$'s surface suggest that CFA particles were successfully incorporated into CHT-ECH molecular structure. Based on the EDX analysis, the major elements contained in the polymeric matrix of CHT-ECH/CFA$_{25}$ were C, O, Si, N, Zr and Cl. After the uptake of RR120, the surface of CHT-ECH/CFA$_{50}$ appeared to be less porous and more compact with fewer cavities (Fig. 3c). This observation can be assigned to the loading of RR120 dye molecules on the CHT-ECH/CFA's surface. Moreover, the presence of S element on EDX analysis reconfirmed the successful capturing of the RR120 dye molecules on the CHT-ECH/CFA$_{50}$ surface.

ANOVA and Empirical Model Fit Equations

The statistical evaluation for input effective variables (A, B, C, D, E) and their response (Y) for this study was performed using ANOVA test and shown in Table 4. It may be observed from Table 4, that F-value is 23.47, and p-value of the quadratic model is < 0.0001, showing this model is highly significant. The significant terms of the model were found to be AB, BD, CD, DE, A^2, D^2 and E^2 denoted by an asterisk (*) in Table 4. Moreover, the high values of determination coefficient (R^2) of 0.9506 and adjusted determination coefficient (R^2 Adj) of 0.911 indicate that the actual and predicted values are highly dependent and correlated [29]. The F-value of the Lack of Fit (LOF) of 2.68 indicates that the LOF is relatively low in comparison to the absolute error. This test shows that the model can accurately deduce the data behavior in the investigated experimental area [29]. The low value (12.68%) of coefficient of variation (C.V.) for RR 120 removal (%) reconfirmed the precision, higher reliability, and excellent reproducibility of the given quadratic model equation [38]. The full quadratic regression model for the RR120 removal (%) using BBD based on Eq. 1 is given in Eq. 4 along with the statistical variables obtained from the ANOVA test.

$$
\begin{aligned}
\text{RR120 removal (\%)} =\ & +31.13 + 18.22A + 9.84B \\
& - 12.15C + 7.56D + 5.42E + 8.23AB \\
& + 5.48\,BD - 5.80CD - 6.80DE \\
& + 12.72\,A2 + 5.99D2 + 5.54E2
\end{aligned}
$$

(4)

The positive and negative signs of the coefficients in the equation indicate the synergistic and antagonistic effects of the variables on the response [2].

Diagnostic of the Responses

The normality of the data was assessed using a normal probability plot and all the data points are relatively close to the diagonal line as shown in Fig. 4a. As the data points were
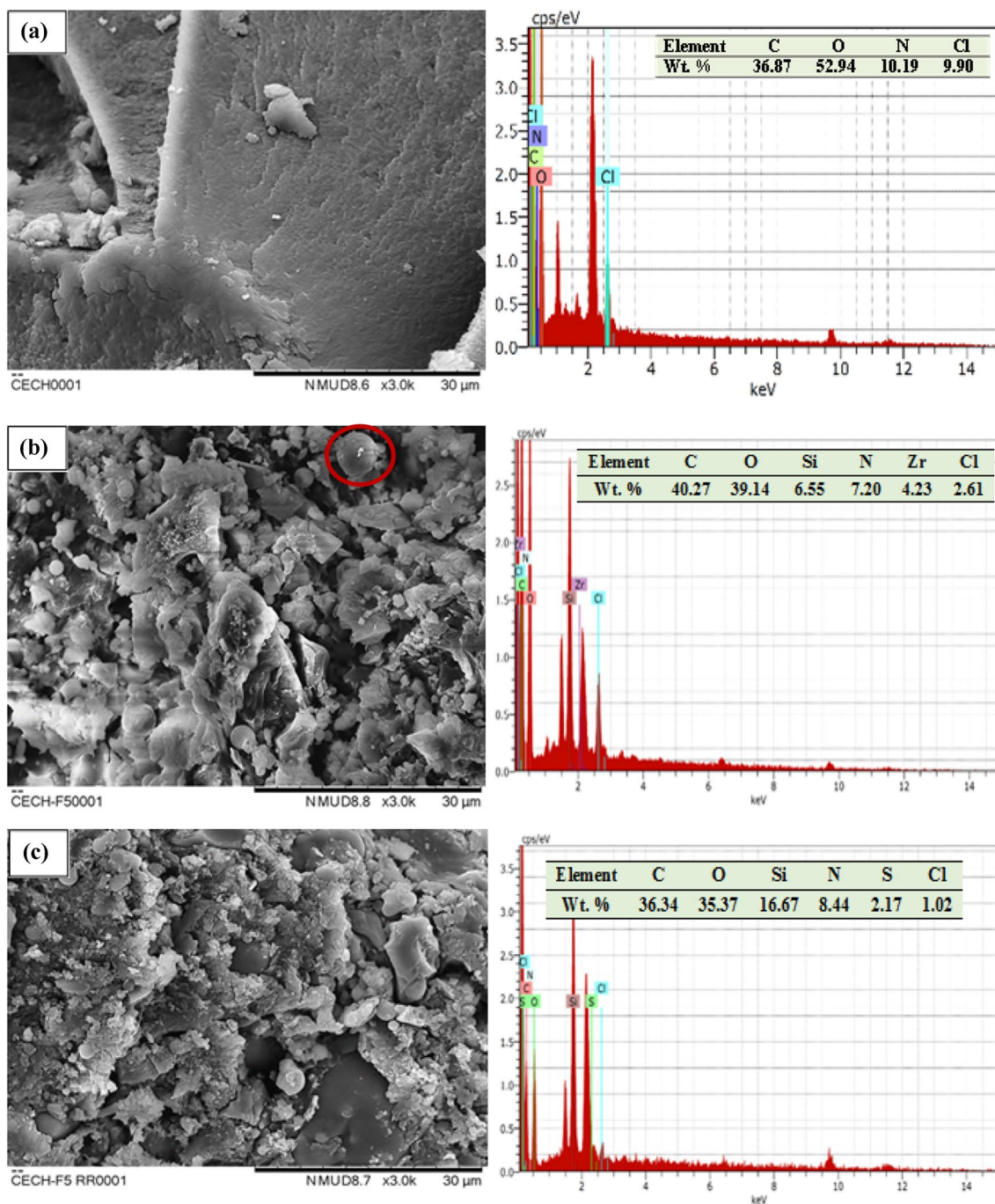
Fig. 3 SEM images of **a** CHT-ECH, **b** CHT-ECH/CFA$_{50}$, **c** CHT-ECH/CFA$_{50}$ after adsorption of RR120 dye at magnification power = 3000×.

distributed along the diagonal line indicating that the errors were normally distributed with mean zero and constant [39]. The relationship between predicted values and actual values of the response is expressed in Fig. 4b. The actual values are depicted by square dots in this plot, whereas the predicted values are represented by a straight line, indicating that there was good agreement between the predicted and actual values for the response. This observation shows that the data is well presented into the model and reconfirmed its suitability to carry out the optimization operation of the process [40]. The plot of residuals versus the predicted values of the response is presented in Fig. 4c, while the plot of the studentized residuals versus run is presented in Fig. 4d. From Fig. 4c and d the adequacy can be predicted and the random scattering of the residuals around zero reveal that the model was well presented, and the constant variance assumption was appropriate [41].

Table 4 Analysis of variance (ANOVA) for the RR120 removal (%)

Source	Sum of Squares	df	Mean Square	F-value	p-value
Model	13056.44	20	652.82	23.47	< 0.0001*
A-CFA loading (%)	5310.77	1	5310.77	190.95	< 0.0001*
B-Dose	1415.64	1	1415.64	50.90	< 0.0001*
C-pH	2535.12	1	2535.12	91.15	< 0.0001*
D-Temp	913.55	1	913.55	32.85	< 0.0001*
E-Time	469.81	1	469.81	16.89	0.0004*
AB	167.70	1	167.70	6.03	0.0214*
AC	104.04	1	104.04	3.74	0.0645
AD	19.36	1	19.36	0.6961	0.4120
AE	67.24	1	67.24	2.42	0.1325
BC	36.00	1	36.00	1.29	0.2660
BD	119.90	1	119.90	4.31	0.0483*
BE	46.92	1	46.92	1.69	0.2058
CD	134.56	1	134.56	4.84	0.0373*
CE	3.61	1	3.61	0.1298	0.7217
DE	184.96	1	184.96	6.65	0.0162*
A^2	1411.78	1	1411.78	50.76	< 0.0001*
B^2	78.65	1	78.65	2.83	0.1051
C^2	70.58	1	70.58	2.54	0.1237
D^2	312.66	1	312.66	11.24	0.0025*
E^2	267.41	1	267.41	9.62	0.0047*
Residual	695.29	25	27.81		
Lack of Fit	637.40	20	31.87	2.75	0.1325
Pure Error	57.89	5	11.58		
Cor Total	13751.73	45			

*Significant

Consequently, the plot of the Cook's distance is presented in Fig. 4e. Generally, the acceptable Cook's distance should be less than 1 [42]. As presented in Fig. 4e, all the observed values are less than 1. Moreover, all 46 runs are even below 0.4 and mainly equal to zero which indicates the significant effect on the predictive power of the model. Consequently, the Box-Cox plot for power transforms plot is presented in Fig. 4f. This graph indicates the most appropriate power transformation to apply for the response values. Hence, the best transformation should be closest to the ideal lambda value (the minimum point of the curve) contains 1 and lies inside the confidence interval. Thus, there is no specific transformation recommended for this BBD-RSM model [43].

Model Graphs for Factors Plot

The model graphs for each independent factor are presented in Fig. 5. It was observed that the loading of CFA (%) in the polymeric matrix of CHT-ECH has a very desirable effect on the output response (RR120 removal (%)), and RR120 removal increased remarkably by increasing the CFA loading as shown in Fig. 5a. Moreover, it seems to be the most dominant input factor over other input factors as presented in Fig. 5a. Moreover, similar trend can be observed with the adsorbent (CHT-ECH/CFA$_{50}$) dose towards the output response (RR120 removal (%)) as shown in Fig. 5b, and comparatively less steep than the loading of CFA (%) curve of Fig. 5a. In contrast, Fig. 5c indicates that the solution pH has a very significant impact on the output response, and the RR120 removal (%) reduced significantly by rising the solution pH towards basic environment (the reason why will be given in the following section). Subsequently, the effect of the working temperature and contact time factors on the output response is illustrated in Fig. 1d and e, respectively. As can be seen, both input factors behaved similarly, and RR120 removal (%) increased by increasing the working temperature and extending the contact time.

Three-Dimensional (3-D) Surface Plots

The 3-dimensional response plots of the independent factors such as A (CFA loading (%)), B (dose), C (pH), D (temperature) and E (time) on the output response (RR120 removal %) are presented in Fig. 6. Hence, Fig. 6a depicts the interactive effect of CFA loading (%) (A) and dose (B) with p-value of 0.0214 which is statistically significant as proven

Fig. 4 Diagnosis plot for developed empirical model equations for RR120 removal (%) **a** normal (%) probability of the residuals, **b** actual versus predicted, **c** residual versus predicated, **d** residual versus run, **e** Cook's distance plot for each of the experimental run, and **f** Plot of box cox for power transform
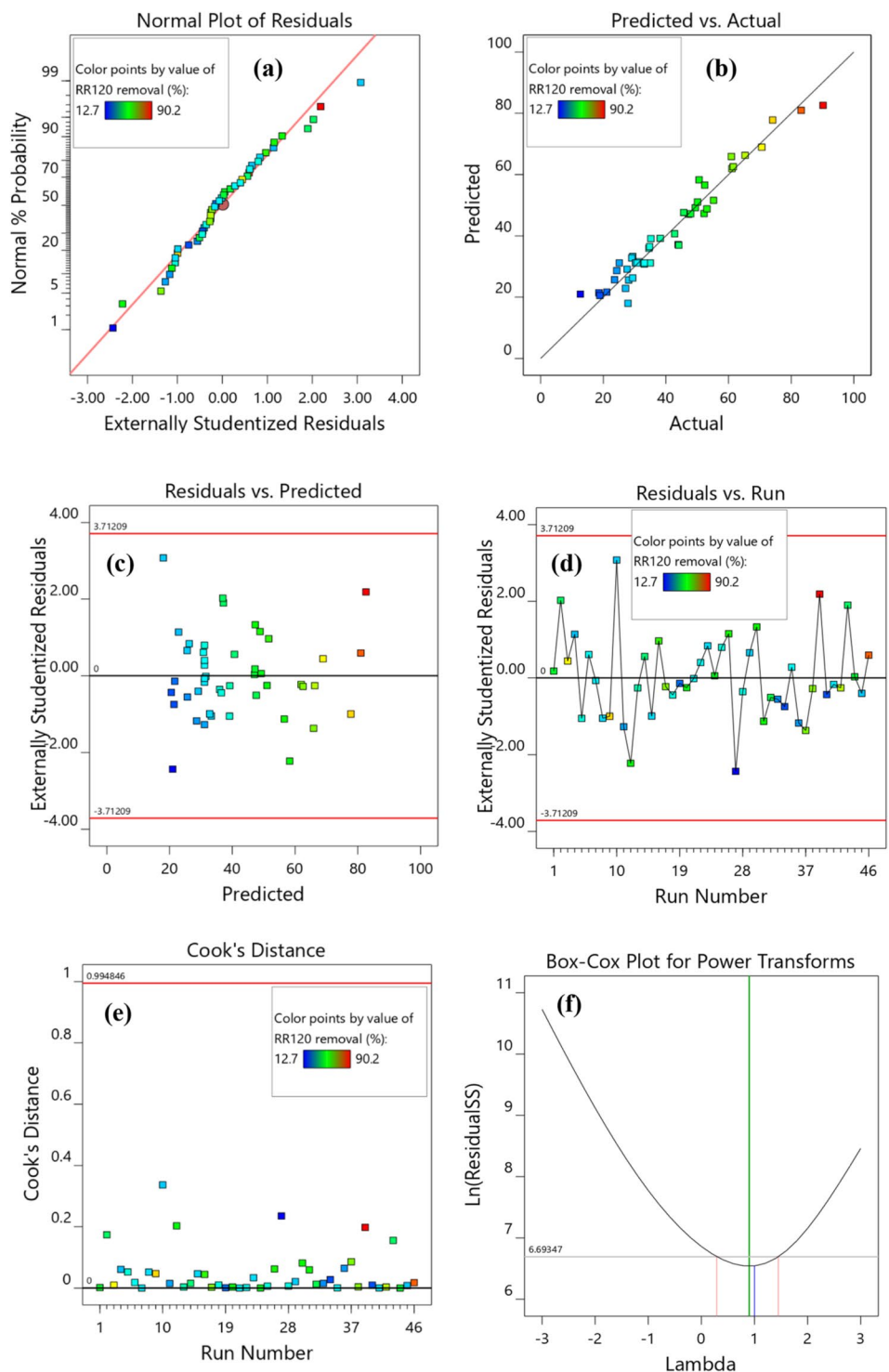
by ANOVA test (Table 4). The efficiency of CHT-ECH/CFA$_{50}$ to remove RR120 (%) elevated from 12.7 to 90.2% as the dose increases from 0.04 to 0.10 g and the increase of CFA loading from 0 to 50%. This observation can be assigned to the uniform distribution of the CFA micro particles in the polymeric matrix of CHT-ECH, and as a result the specific surface area and pore diameter of CHT-ECH/CFA$_{50}$ were developed and enhanced as proven in Table 3. This enhanced surface area property will lead to efficient diffusion of the RR120 dye molecules into inter pores and/or adsorption active sites. Subsequently, adding more doses of the adsorbent (CHT-ECH/CFA$_{50}$) to the dye solution will offer more active adsorption sites for capturing anionic dye molecules such as RR120 [44]. Besides that, the interaction
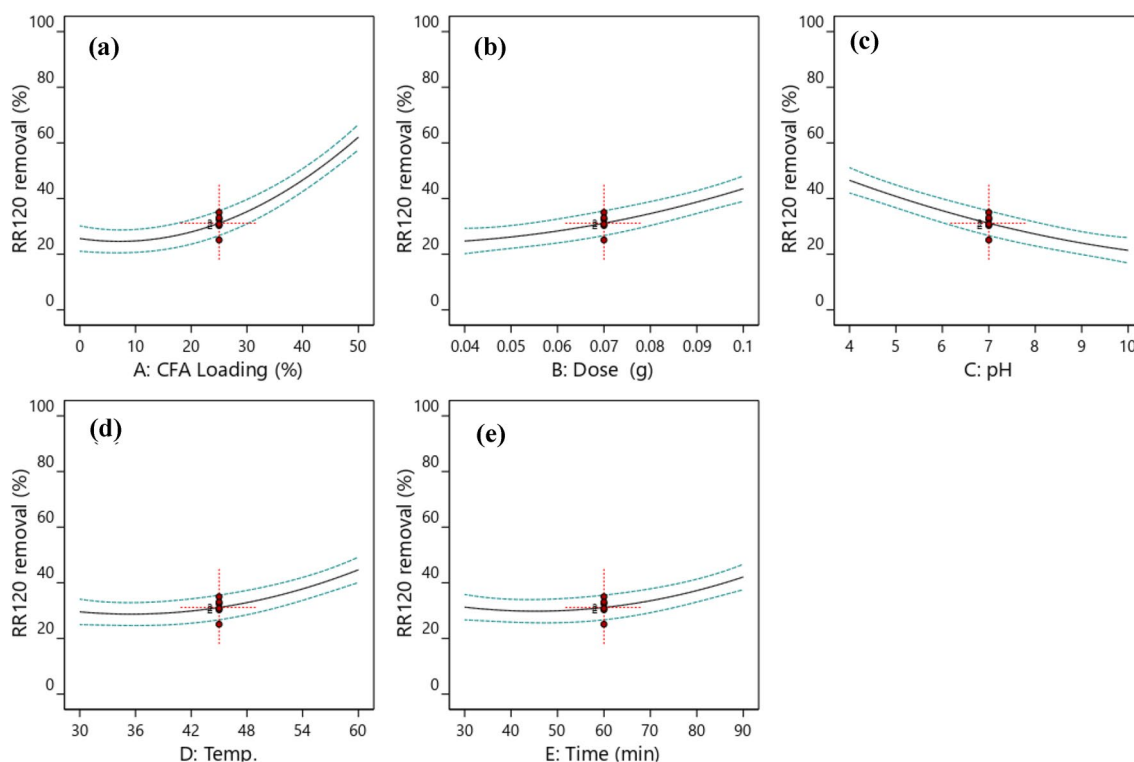
Fig. 5 Effect of individual input variable on the output response (RR120 removal (%), **a** CFA loading (%), **b** adsorbent dose, **c** solution pH, **d** working temperature, and **e** contact time.

between dose (B) and temperature (D) was observed to be statistically significance with p-value of 0.0483. It can be confirmed from Fig. 6b, the removal of RR120 (%) significantly improves as the temperature increases from 30ºC to 60 °C. This result shows that the process of RR120 removal (%) by CHT-ECH/CFA$_{50}$ is an endothermic in nature. A similar trend can be observed from Fig. 6c and d where the RR120 removal (%) increases as the temperature increases. Furthermore, the relationship between input variables of working temperature (D) and contact time (E) on the output response was investigated and presented in Fig. 6d. The interaction is statistically significant as indicated by p-value (0.0162) from Table 4. As can be seen from solo input variable (Fig. 5c) and reconfirmed in the significant interaction of input variables (Fig. 6c), the RR120 removal (%) is very sensitive to the solution pH change. In this respect, it can be observed clearly that the RR120 removal (%) was greater in acidic pH range and decreased with an increase in solution pH towards basic environment. The acidity of the medium is a significant factor affecting the RR120 adsorption onto CHT-ECH/CFA$_{50}$ surface. This could be due to the change in surface charge of the adsorbent explained by pH$_{pzc}$ as displayed in Table 3, as the value of pH$_{pzc}$ was found to be 7.1. This observation demonstrates that the CHT-ECH/CFA$_{50}$ is a positively charged adsorbent at acidic environment due to the protonation of –NH$_2$ into –NH$_3^+$ group, which is very

much preferable in capturing anionic dye molecules from treated solution [32–34].

The Effect of Contact Time and Kinetic Study

The influence of contact time on RR120 adsorption at various initial concentrations (50–300 mgL) was investigated by adopting the optimal input variables' values which were previously determined from experiment 14 in Table 2 as follows: CHT-ECH/CFA$_{50}$ = 0.07 g, solution pH = 4, and working temperature = 45 ºC. Figure 7a shows the RR120 uptake by CHT-ECH/CFA$_{50}$ versus contact time at different initial RR120 concentrations. As can be seen, the adsorption occurred quickly in the initial steps due to availability of unoccupied adsorption active sites, and then gradually filled over time, resulting in no more change in adsorption capacity [8, 35]. The adsorption kinetics were determined by applying Lagergren pseudo-first order (PFO) model [45] and pseudo-second order (PSO) model [46]. The non-linear forms of these PFO and PSO models can be expressed in the Eqs. 5 and 6 respectively.

$$q_t = q_e \left(1 - \exp^{-k_1 t}\right) \tag{5}$$
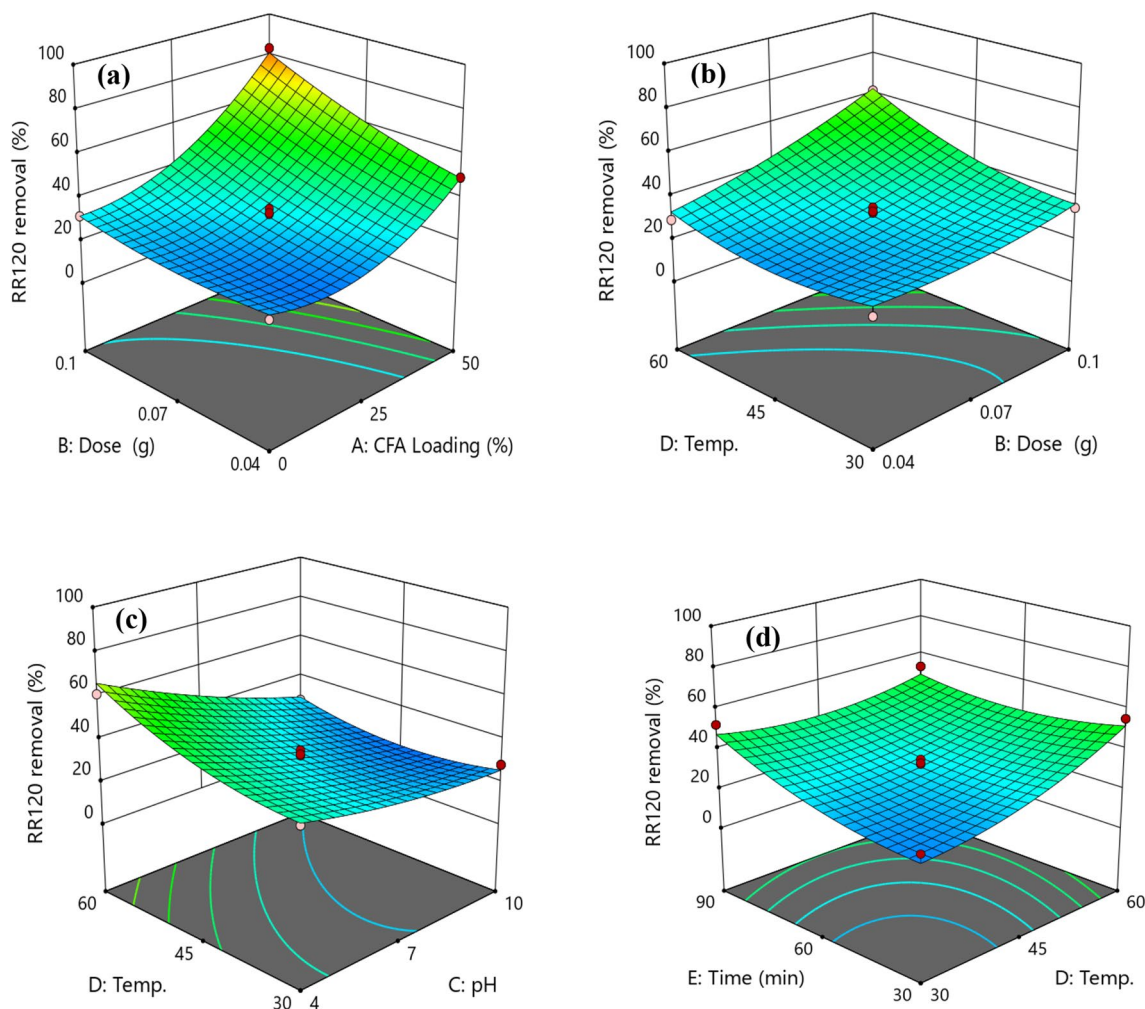
Fig. 6 3D plots of significant interaction between input variables on the output response (RR120 removal %) as shown in **a** AB, **b** BD, **c** CD and **d** DE

$$q_t = \frac{q_e^2 k_2 t}{1 + q_e k_2 t} \tag{6}$$

where, q_t (mg/g) is the amount of RR120 adsorbed by CHT-ECH/CFA$_{50}$ at time and q_e (mg/g) is the amount of RR120 uptake by CHT-ECH/CFA$_{50}$ at equilibrium. k_1 (1/min) and k_2 (g/mg min) are the corresponding rate constants of the two models, respectively. Table 4 presents the correlation coefficients (R^2) of the kinetic parameters of these models, which depicts that the adsorption kinetic is well described by PSO rather than PFO kinetic model. Moreover, the calculated q_e values of PSO model are very close to the experimental q_e values. The dominancy of the PSO over PFO indicates that the overall rate of the adsorption process was controlled by chemisorption which involves valency forces through electrons sharing between the adsorbent and adsorbate [47].

Adsorption Isotherm

Adsorption isotherm is an important function to investigate the most appropriate adsorption isotherms for predicting the pathways of the adsorption mechanism of RR120 onto CHT-ECH/CFA$_{50}$. The isotherm parameters obtained will aid in understanding the adsorbent/adsorbate interactions [48]. Thus, many isotherm models such as Langmuir model [49], Freundlich model [50] and Temkin model [51] were used in this study. The Langmuir model is a typically adopted adsorption isotherm that portrays the mechanism of monolayer adsorption on a defined homogeneous surface. The nonlinear Langmuir isotherm equation is expressed in Eq. 7.

$$q_e = \frac{q_{max} K_a C_e}{1 + K_a C_e} \tag{7}$$
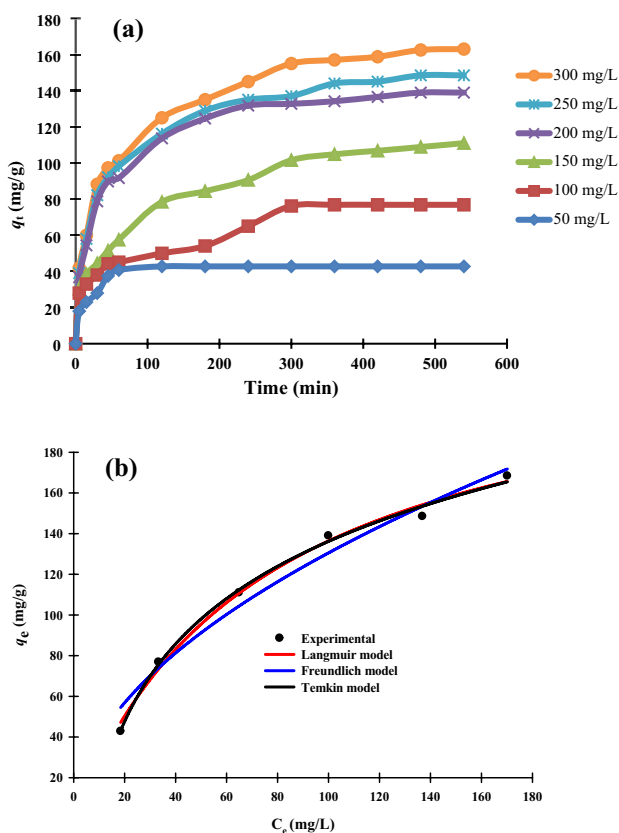
Fig. 7 **a** Effect of the contact time on RR120 adsorption at different initial concentrations, and **b** adsorption isotherms of RR120 by CHT-ECH/CFA$_{50}$ at the following experimental condition: (dosage 0.07 g, pH of solution 4, temperature 45 °C, agitation speed = 100 strokes/min, and volume of solution = 100 mL).

where q_e and C_e represent the amount of RR120 adsorbed at equilibrium (mg/g) and the equilibrium RR120 concentration (mg/L). q_{max} is the maximum adsorbed quantity of RR120 (mg/g) and K_a is the Langmuir constant related to the active adsorption sites affinity (L/mg). Conversely, the Freundlich isotherm is an empirical equation which is applicable for adsorption processes occurring on heterogeneous sites with different adsorption energies [50]. The empirical

description of the Freundlich isotherm model is given in Eq. 8.

$$q_e = K_f C_e^{1/n} \tag{8}$$

where the Freundlich constant K_f is related to the adsorption capacity (mg/g) and n provides the information regarding the adsorption process's favourability (Table 5). The Temkin model is based on the presumption that as the coverage increases, the adsorption energy reduces linearly [51]. The Temkin isotherm can be described in Eq. 9.

$$q_e = \frac{RT}{b_T} \ln(K_T C_e) \tag{9}$$

where R (J/mol K) is the universal gas constant (8.314), T (K) is temperature, the Temkin constants b_T is associated to the heat of adsorption and K_T (L/mg) is the constant related to the equilibrium binding. The plots of the adsorption isotherm models are presented in Fig. 7b and their corresponding parameters computed based on the models are summarized in Table 6. It shows that higher correlation coefficient values were obtained for both Langmuir model ($R^2 = 0.99$) and Freundlich model ($R^2 = 0.98$), implying a homogeneous and heterogeneous mode of adsorption. The maximum monolayer adsorption capacity (q_{max}) of CHT-ECH/CFA$_{50}$ computed from the Langmuir model is 237.7 mg/g. In addition, higher K_f value (12.1) and the value of n which is greater than 1 (n = 1.29), suggest that the adsorption process is favourable [52]. Moreover, the adsorption capacity of CHT-ECH/CFA$_{50}$ alongside various adsorbents towards RR210 dye was assessed, and the summary of the adsorption capacities are presented in Table 7. Thus, the reported data indicates that CHT-ECH/FA$_{50}$ can be considered as a potential low-cost adsorbent for treatment of acidic (anionic) dye in the aqueous environment.

Adsorption Thermodynamic

Thermodynamic study was carried out to navigate the thermodynamic functions that derive the adsorption process of RR210 onto CHT-ECH/CFA$_{50}$ surface. The following

Concentration (mg/L)	$q_{e\,exp}$ (mg/g)	PFO			PSO		
		$q_{e\,cal}$ (mg/g)	k_1 (1/min)	R^2	$q_{e\,cal}$ (mg/g)	$k_2 \times 10^{-3}$ (g/mg min)	R^2
50	42.8	42.5	0.051	0.95	44.4	2.09	0.97
100	76.9	70.4	0.022	0.81	77.6	0.41	0.99
150	111.0	102.5	0.016	0.92	116.2	0.17	0.96
200	138.9	131.8	0.027	0.96	143.4	0.27	0.99
250	148.5	138.6	0.026	0.95	151.2	0.25	0.98
300	163.0	151.6	0.024	0.94	167.0	0.20	0.98

Table 5 PFO and PSO kinetic parameters for RR120 adsorption on CHT-ECH/CFA$_{50}$ at 45 °C

Table 6 Parameters of the Langmuir, Freundlich and Temkin isotherm models for RR120 adsorption by CHT-ECH/CFA$_{50}$ at 45 ºC

Adsorption isotherm	Parameter	Value
Langmuir	q_{max} (mg/g)	237.7
	K_a (L/mg)	0.013
	R^2	0.99
Freundlich	K_f (mg/g) (L/mg)$^{1/n}$	12.1
	n	1.29
	R^2	0.98
Temkin	K_T (L/mg)	55.1
	b_T (J/mol)	44.9
	R^2	0.95

Table 7 Comparison adsorption capacities of various adsorbents for RR120

Adsorbents	q_{max} (mg/g)	References
Crosslinked chitosan-iron (III)	361.9	[53]
Modified orange peel powder	344.8	[3]
Commercial activated carbon	267.2	[54]
CHT-ECH/CFA$_{50}$	237.7	This study
Crosslinked chitosan-nano TiO$_2$	210.0	[55]
Schiff's base- chitosan-nano TiO$_2$	103.1	[33]
Treated *Jatropha curcas* shells	85.3	[56]
Cross-linked chitosan epichlorohydrin	81.3	[57]
Thermally treated sewage sludge	46.8	[58]

Table 8 Thermodynamic parameters for the adsorption of RR120 dye by CHT-ECH/CFA$_{50}$

T (K)	k_d	$\Delta G°$ (kJ/mol)	$\Delta H°$ (kJ/mol)	$\Delta S°$ (kJ/molK)
303.15	2.18	−1.96	71.73	0.24
313.15	5.40	− 4.39		
323.15	9.55	− 6.06		
333.15	31.95	− 9.60		

$$y = -8627.6x + 29.223$$
$$R^2 = 0.9816$$

Fig. 8 Van't Hoff plot RR120 dye adsorption onto CHT-ECH/FA$_{50}$ (dosage = 0.07 g, pH of solution = 4, agitation speed = 100 strokes and volume of solution = 100 mL).

Eqs. (10), (11), and (12) were applied to compute the standard change for Gibb's free energy $\Delta G°$ (kJ/mol), enthalpy $\Delta H°$ (kJ/mol) and entropy $\Delta S°$ (kJ/mol K), respectively.
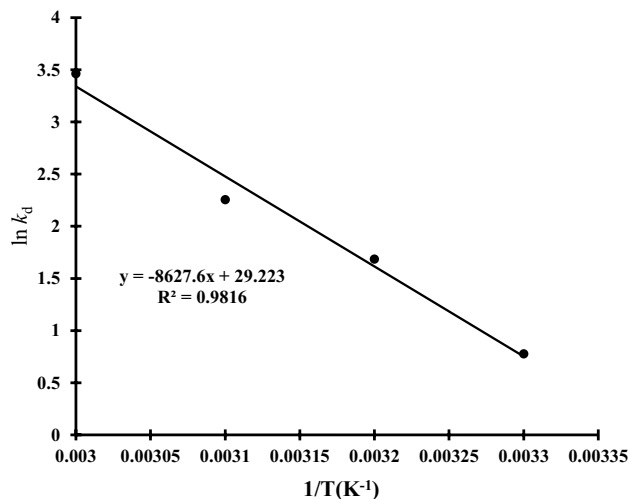
$$\Delta G° = -RT\ln k_d \qquad (10)$$

$$k_d = \frac{q_e}{C_e} \qquad (11)$$

$$\ln k_d = \frac{\Delta S°}{R} - \frac{\Delta H°}{RT} \qquad (12)$$

where T is the absolute temperature and R is the universal gas constant (8.314 J/mol K). k_d is the distribution coefficient, q_e is the amount of dye adsorbed by CHT-ECH/CFA$_{50}$ at equilibrium (mg/g) and C_e is the equilibrium dye concentration in the liquid phase (mg/L). The calculated thermodynamic parameters are presented in Table 8 and from the gradient and intercept of Van't Hoff plots of $\ln k_d$ against 1/T (Fig. 8), the values of $\Delta H°$ and $\Delta S°$ were computed respectively. Based on the thermodynamic calculations, the uptake of RR120 at solution pH 4 onto CHT-ECH/CFA$_{50}$ surface was indicated as a spontaneous process if the value of Gibbs energy change ($\Delta G°$) at all working temperatures

were negative. In addition, as the temperature increases, $\Delta G°$ decreases, implying a stronger adsorption force and thus promoting the adsorption spontaneity to occur at high temperature [47]. The entropy change ($\Delta S°$) is positive (0.24 kJ/mol K) which signifies an enhancement of the system randomness at the solid/solution interface during the adsorption process. The positive enthalpy change ($\Delta H°$ = 71.37 kJ/mol) advocates an endothermic nature and suggesting that energy is required in transferring RR120 from the aqueous phase to the solid phase [59].

Adsorption Mechanism

The proposed mechanism for the adsorption of RR120 dye onto CHT-ECH/CFA$_{50}$ is illustrated in Fig. 9. CHT contains large amounts of amino (–NH$_2$) and hydroxyl (–OH) functional groups, making it an ideal adsorbent for removing anionic pollutants from the aqueous systems. These amino (–NH$_2$) groups can easily be protonated (–NH$_3^+$) in acidic medium, enabling them to strongly adsorb anionic dyes through strong electrostatic attractions [1, 5]. Other possible forces are dipole-dipole hydrogen bonding and Yoshida
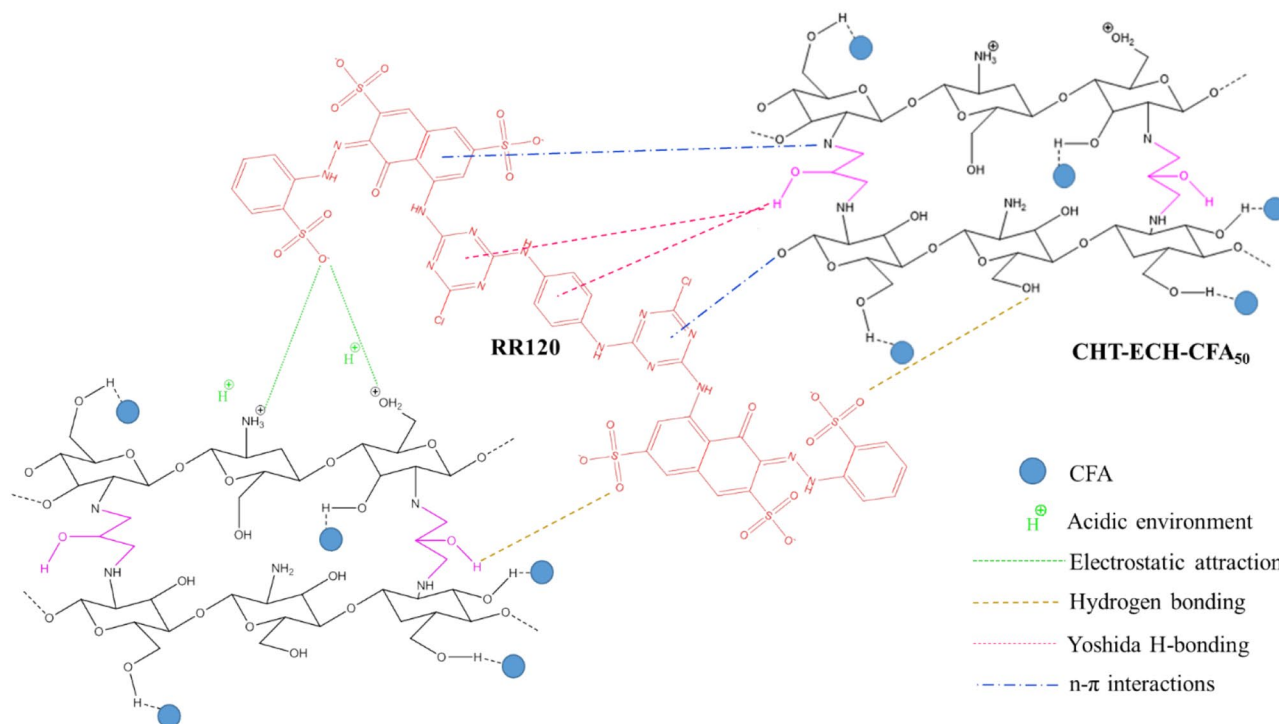
Fig. 9 Illustration of the possible interaction between CHT-ECH/CFA$_{50}$ surface and RR120 dye including electrostatic attraction, hydrogen bonding interactions, Yoshida H-bonding, and n-π interactions

H-bonding which can be formed by the interaction of existing H and –OH on the CHT-ECH/CFA$_{50}$ surface with nitrogen (N) atom in the aromatic ring of RR120 dye structure [8, 29]. Furthermore, possible n-π stacking interactions can be formed between the delocalization of lone pair electrons on an oxygen (O) atom and nitrogen (N) atom into the π orbital in the aromatic ring of the RR120 [33, 35].

Conclusions

Synthesis of the CHT-ECH/CFA was performed, and it was applied for removing RR120 dye from aquatic environment. Box-Behnken design model was applied in order to investigate the impact of four independent factors such as CFA loading, dose, temperature, pH and time on the removal of RR120 dye. The experimental data were interpreted using the second-order polynomial regression model, which had a coefficient of determination R^2 value of 0.95 and F-value of 24.04, and the maximum adsorption of RO16 was estimated to be up to 90.2% within the range studied. The quadratic model fit the experimental data well based on the p-value obtained. The optimal conditions obtained for the RR120 removal were 50% CFA loading, 0.07 g of adsorbent dose, pH solution of 4, and working temperature (45 °C). The isotherm data fit best with Langmuir isotherm model and

the q_{max} computed by Langmuir isotherm was 237.7 mg/g. Kinetic experimental data demonstrated that the process of the adsorption followed pseudo-second order kinetics.

Declarations

Conflict of interest The authors declare that there is no conflict of interest.

References

1. Reghioua A, Barkat D, Jawad AH, Abdulhameed AS, Rangabhashiyam S, Khan MR, ALOthman ZA (2021) Magnetic chitosan-glutaraldehyde/Zinc Oxide/Fe$_3$O$_4$ nanocomposite: Optimization and adsorptive mechanism of Remazol Brilliant Blue R Dye Removal. J Polym Environ 29:3932–3947

2. Shukla SK, Pandey S, Saha S, Singh HR, Mishra PK, Kumar S, Jha SK (2021) Removal of crystal violet by Cu-chitosan nano-bio-composite particles using box-behnken design. J Environ Chem Eng 9(5):105847–105862

3. Munagapati VS, Wen JC, Pan CL, Gutha Y, Wen JH (2019) Enhanced adsorption performance of reactive red 120 azo dye from aqueous solution using quaternary amine modified orange peel powder. J Mol Liq 285:375–385

4. Munagapati VS, Wen HY, Wen JC, Gollakot ARK, Shu CM, Reddy GM (2021) Characterization of protonated amine modified lotus (*Nelumbo nucifera*) stem powder and its application in the removal of textile (Reactive Red 120) dye from liquid phase. J Mol Liq 338:116486–116501

5. Mokhtar A, Abdelkrim S, Djelad A, Sardi A, Boukoussa B, Sassi M, Bengueddach A (2020) Adsorption behavior of cationic and anionic dyes on magadiite-chitosan composite beads. Carbohydr Polym 229:115399–115408

6. Pitchay T, Jawad AH, Johari IS, Sabar S (2022) Kinetic study of metal ions adsorption by immobilised chitosan. Sci Lett 16(1):137–148

7. Vakili M, Qiu W, Cagnetta G, Huang J, Yu G (2021) Mechanochemically oxidized chitosan-based adsorbents with outstanding Penicillin G adsorption capacity. J Environ Chem Eng 9:105454–105465

8. Abdulhameed AS, Mohammad AT, Jawad AH (2019) Modeling and mechanism of reactive orange 16 dye adsorption by chitosan-glyoxal/TiO_2 nanocomposite: application of response surface methodology. Desalin Water Treat 164:346–360

9. Zhang M, Zhang Z, Peng Y, Feng L, Li X, Zhao C, Sarfaraz K (2020) Novel cationic polymer modified magnetic chitosan beads for efficient adsorption of heavy metals and dyes over a wide pH range. Int J Biol Macromol 156:289–301

10. Jawad AH, Sahu UK, Jani NA, ALOthman ZA, Wilson LD (2022) Magnetic crosslinked chitosan-tripolyphosphate/MgO/Fe_3O_4 nanocomposite for reactive blue 19 dye removal: Optimization using desirability function approach. Surf Interfaces 28:101698–101710

11. Salama A, Abou-Zeid RE (2021) Ionic chitosan/silica nanocomposite as efficient adsorbent for organic dyes. Int J Biol Macromol 188:404–410

12. Şenol ZM, Çetinkaya S, Yenidünya AF, Başoğlu-Ünal F, Ece A (2022) Epichlorohydrin and tripolyphosphate-crosslinked chitosan–kaolin composite for Auramine O dye removal from aqueous solutions. Experimental study and DFT calculations. Int J Biol Macromol 199:318–330

13. Reghioua A, Barkat D, Jawad AH, Abdulhameed AS, Khan MR (2021) Synthesis of Schiff's base magnetic crosslinked chitosan-glyoxal/ZnO/Fe_3O_4 nanoparticles for enhanced adsorption of organic dye: Modeling and mechanism study. Sustain Chem Pharm 20:100379–100394

14. Zhang C, Chen Z, Guo W, Zhu C, Zou Y (2018) Simple fabrication of chitosan/graphene nanoplates composite spheres for efficient adsorption of acid dyes from aqueous solution. Int J Biol Macromol 112:1048–1054

15. Malek NNA, Mohammad IA, Reghioua A, Yousif E, Jawad AH (2020) Removal of reactive red 4 dye using chitosan-epichlorohydrin/ TiO_2 nanocomposite: application of response surface methodology. Sci Lett 14(1):96–108

16. Yu X, Zhang J, Zheng Y (2021) Perchlorate adsorption onto epichlorohydrin crosslinked chitosan hydrogel beads. Sci Total Environ 761:143236–143245

17. Xu Z, Wang X, Sun S (2021) Performance of a synthetic resin for lithium adsorption in waste liquid of extracting aluminum from fly-ash. Chin J Chem Eng 44:115–123

18. Qiu Q, Jiang X, Lv G, Chen Z, Lu S, Ni M, Yan J, Deng X (2018) Adsorption of heavy metal ions using zeolite materials of municipal solid waste incineration fly ash modified by microwave-assisted hydrothermal treatment. Powder Technol 335:156–163

19. Ramanathan S, Gopinath SC, Arshad MM, Poopalan P (2020) Nanostructured aluminosilicate from fly ash: Potential approach in waste utilization for industrial and medical applications. J Clean Prod 253:119923–119938

20. Nazari E, Rashchi F, Saba M, Mirazimi S (2014) Simultaneous recovery of vanadium and nickel from power plant fly-ash: Optimization of parameters using response surface methodology. Waste Manage 34:2687–2696

21. de Carvalho T, Fungaro D, Magdalena C, Cunico P (2011) Adsorption of indigo carmine from aqueous solution using coal fly ash and zeolite from fly ash. J Radioanal Nucl Chem 289:617–626

22. Ochedi FO, Liu Y, Hussain A (2020) A review on coal fly ash-based adsorbents for mercury and arsenic removal. J Clean Prod 267:122143–122158

23. Yuan Y, Zhang H, Pan G (2016) Flocculation of cyanobacterial cells using coal fly ash modified chitosan. Water Res 97:11–18

24. Zang L, Qiao X, Hu L, Yang C, Liu Q, Wei C, Qiu J, Mo H, Song G, Yang J, Liu C (2018) Preparation and evaluation of coal fly ash/chitosan composites as magnetic supports for highly efficient cellulase immobilization and cellulose bioconversion. Polymers 10(5):523–535

25. Mu C, Zhang L, Zhang X, Zhong L, Li Y (2020) Selective adsorption of Ag (I) from aqueous solutions using chitosan/polydopamine@C@magnetic fly ash adsorbent beads. J Hazard Mater 381:120943–120953

26. Adamczuk A, Kołodyńska D (2015) Equilibrium, thermodynamic and kinetic studies on removal of chromium, copper, zinc and arsenic from aqueous solutions onto fly ash coated by chitosan. Chem Eng J 274:200–212

27. Agarwal S, Rajoria P, Rani A (2018) Adsorption of tannic acid from aqueous solution onto chitosan/NaOH/fly ash composites: Equilibrium, kinetics, thermodynamics and modeling. J Environ Chem Eng 6(1):1486–1499

28. Mohammed IA, Jawad AH, Abdulhameed AS, Mastuli MS (2020) Physicochemical modification of chitosan with fly ash and tripolyphosphate for removal of reactive red 120 dye: Statistical optimization and mechanism study. Int J Biol Macromol 161:503–513

29. Malek NNA, Jawad AH, Ismail K, Razuan R, ALOthman ZA (2021) Fly ash modified magnetic chitosan-polyvinyl alcohol blend for reactive orange 16 dye removal: Adsorption parametric optimization. Int J Biol Macromol 189:464–476

30. Vieira RS, Beppu MM (2006) Interaction of natural and crosslinked chitosan membranes with Hg (II) ions, Colloids Surf. A Physicochem Eng Asp 279:196–207

31. Dalvand A, Nabizadeh R, Ganjali MR, Khoobi M, Nazmara S, Mahvi AH (2016) Modeling of reactive blue 19 azo dye removal from colored textile wastewater using l-arginine-functionalized Fe_3O_4 nanoparticles: Optimization, reusability, kinetic and equilibrium studies. J Magn Magn Mater 404:179–189

32. Montgomery DC (2017) Design and Analysis of Experiments, 8th edn. Wiley, New York

33. Jawad AH, Mubarak NSA, Abdulhameed AS (2020) Tunable Schiff's base-cross-linked chitosan composite for the removal of reactive red 120 dye: Adsorption and mechanism study. Int J Biol Macromol 142:732–741

34. Jawad AH, Malek NNA, Abdulhameed AS, Razuan R (2020) Synthesis of magnetic chitosan-fly ash/Fe_3O_4 composite for adsorption of reactive orange 16 dye: Optimization by box–behnken design. J Polym Environ 28:1068–1082

35. Jawad AH, Abdulhameed AS, Reghioua A, Yaseen ZM (2020) Zwitterion composite chitosan-epichlorohydrin/zeolite for adsorption of methylene blue and reactive red 120 dyes. Int J Biol Macromol 163:756–765

36. Saratale RG, Sun Q, Munagapati VS, Saratale GD, Park J, Kim DS (2021) The use of eggshell membrane for the treatment of dye-containing wastewater: Batch, kinetics and reusability studies. Chemosphere 281:130777–130786

37. Habiba U, Siddique TA, Joo TC, Salleh A, Ang BC, Afifi AM (2017) Synthesis of chitosan/polyvinyl alcohol/zeolite composite for removal of methyl orange, congo red and chromium (VI) by flocculation/adsorption. Carbohydr Polym 157:1568–1576

38. Yadav AM, Chaurasia RC, Suresh N, Gajbhiye P (2018) Application of artificial neural networks and response surface methodology approach for the prediction of oil agglomeration process. Fuel 220:826–836

39. Menkiti MC, Nnaji PC, Onukwuli OD (2009) Coag- flocculation kinetics and functional parameters response of Periwinkle Shell Coagulant (PSC) to pH variation in organic rich coal effluent medium. Nat Sci 7(6):1–18

40. Ezemagu IG, Ejimofor MI, Menkiti MC, Nwobi-Okoye CC (2021) Modeling and optimization of turbidity removal from produced water using response surface methodology and artificial neural network. S Afr J Chem Eng 35:78–88

41. Mostafaloo R, Mahmoudian MH, Asadi-Ghalhari M (2019) $BiFeO_3$/Magnetic nanocomposites for the photocatalytic degradation of cefixime from aqueous solutions under visible light. J Photochem Photobiol A 382:111926–111934

42. Nasri Z, Mozafari M (2018) Multivariable statistical analysis and optimization of Iranian heavy crude oil upgrading using microwave technology by response surface methodology (RSM). J Pet Sci Eng 161:427–444

43. Verma A, Ojha K (2021) Application of response surface methodology for the optimization of viscosity of foam fracturing fluids for the unconventional reservoir. J Nat Gas Sci Eng 94:104086–104098

44. Jaafari J, Barzanouni H, Mazloomi S, Farahani NA, Sharafi K, Soleimani P, Haghighat GA (2020) Effective adsorptive removal of reactive dyes by magnetic chitosan nanoparticles: Kinetic, isothermal studies and response surface methodology. Int J Biol Macromol 164:344–355

45. Lagergren S (1898) Zur theorie der sogenannten adsorption geloster stoffe. Vet Akad Handl 24:1–39

46. Ho YS, McKay G (1998) Sorption of dye from aqueous solution by peat. Chem Eng J 70:115–124

47. Jiang Y, Cai W, Tu W, Zhu M (2018) Facile cross-link method to synthesize magnetic Fe_3O_4@ SiO_2–chitosan with high adsorption capacity toward hexavalent chromium. J Chem Eng Data 64:226–233

48. Habiba U, Siddique TA, Lee JJL, Joo TC, Ang BC, Afifi AM (2018) Adsorption study of methyl orange by chitosan/polyvinyl alcohol/zeolite electrospun composite nanofibrous membrane. Carbohydr Polym 191:79–85

49. Langmuir I (1918) The adsorption of gases on plane surfaces of glass, mica and platinum. J Am Chem Soc 40:1361–1403

50. Freundlich H (1906) Freundlich's Adsorption Isotherm. Phys Chem 57:385–471

51. Temkin M, Pyzhev V (1940) Recent modifications to Langmuir isotherms. Acta Physiochem 12:217–222

52. Habiba U, Lee JJL, Joo TC, Ang BC, Afifi AM (2019) Degradation of methyl orange and congo red by using chitosan/polyvinyl alcohol/ TiO_2 electrospun nanofibrous membrane. Int J Biol Macromol 131:821–827

53. Demarchi CA, Campos M, Rodrigues CA (2013) Adsorption of textile dye reactive red 120 by the chitosan–Fe(III)-crosslinked: batch and fixed-bed studies. J Environ Chem Eng 1(4):1350–1358

54. Cardoso NF, Lima EC, Royer B, Bach MV, Dotto GL, Pinto LA, Calvete T (2012) Comparison of *Spirulina platensis* microalgae and commercial activated carbon as adsorbents for the removal of reactive red 120 dye from aqueous effluents. J Hazard Mater 241:146–153

55. Jawad AH, Mubarak NSA, Abdulhameed AS (2020) Hybrid crosslinked chitosan epichlorohydrin/ TiO_2 nanocomposite for reactive red 120 dye adsorption: kinetic, isotherm, thermodynamic, and mechanism study. J Polym Environ 28:624–637

56. Prola LD, Acayanka E, Lima EC, Umpierres CS, Vaghetti JC, Santos WO, Djifon PT (2013) Comparison of *Jatropha curcas* shells in natural form and treated by nonthermal plasma as biosorbents for removal of reactive red 120 textile dye from aqueous solution. Ind Crop Prod 46:328–340

57. Jawad AH, Mubarak NSA, Sabar S (2019) Adsorption and mechanism study for reactive red 120 dye removal by cross-linked chitosan-epichlorohydrin biobeads, Desalin. Water Treat 164:378–387

58. Pereira IC, Carvalho KQ, Passig FH, Ferreira RC, Rizzo-Domingues RCP, Hoppen MI, Perretto F (2018) Thermal and thermal-acid treated sewage sludge for the removal of dye reactive red 120: characteristics, kinetics, isotherms, thermodynamics and response surface methodology design. J Environ Chem Eng 6(6):7233–7246

59. Ghibate R, Senhaji O, Taouil R (2021) Kinetic and thermodynamic approaches on Rhodamine B adsorption onto pomegranate peel, Case Stud. Chem Environ Eng 3:100078–100083

Publisher's note Springer Nature remains neutral with regard to jurisdictional claims in published maps and institutional affiliations.